WILEY InterScience® DISCOVER SOMETHING GREAT

Restricted and Unrestricted Hartree–Fock Approaches Applied to Spherical Quantum Dots in a Magnetic Field

C. F. DESTEFANI,[1] J. D. M. VIANNA,[2,3] G. E. MARQUES[1]

[1]*Departamento de Física, Universidade Federal de São Carlos, 13565-905 São Carlos-SP, Brazil*

[2]*Instituto de Física, Universidade de Brasília, 70910-900 Brasília-DF, Brazil*

[3]*Instituto de Física, Universidade Federal da Bahia, 40210-340 Salvador-BA, Brazil*

Received 24 December 2004; accepted 12 April 2005
Published online 13 March 2006 in Wiley InterScience (www.interscience.wiley.com).
DOI 10.1002/qua.20984

ABSTRACT: The Roothaan and Pople–Nesbet approaches for real atoms are adapted to quantum dots in the presence of a magnetic field. Single-particle Gaussian basis sets are constructed, for each dot radius, under the condition of maximum overlap with the exact functions. The chemical potential, charging energy, and total spin expected values are calculated, and we have verified the validity of the quantum dot energy shell structure as well as Hund's rule for electronic occupation at zero magnetic field. At finite field, we have observed the violation of Hund's rule and studied the influence of magnetic field on the closed and open energy shell configurations. We have also compared the present results with those obtained within the LS-coupling scheme for low electronic occupation numbers. We focus only on ground-state properties and consider quantum dots populated up to 40 electrons, constructed by GaAs or InSb nanocrystals. Int J Quantum Chem 106: 2090–2099, 2006

Key words: Roothaan–Pople–Nesbet Hartree–Fock; quantum dots; Hund's rule

1. Introduction

The influence of the spatial confinement on the physical properties, such as electronic spectra of nanostructured systems, is a topic of growing interest. Among the several kinds of confined systems, one can detach low-dimensional electronic gases and impurity atoms in metallic or semiconductor mesoscopic structures [1], as well as atoms, ions, and molecules trapped in microscopic cavities [1–5], where the effects of the confinement become important when the typical quantum sizes, such as Fermi wavelength, reach the same order of magnitude as the sizes of the cavities. However, the energy spectrum of such systems is not only determined by the spatial confinement and geometric

Correspondence to: C. F. Destefani; e-mail: carlusfernandus@rogers.com

Contract grant sponsors: Fundação de Amparo à Pesquisa do Estado de São Paulo (FAPESP); Conselho Nacional de Desenvolvimento Científico e Tecnológico (CNPq), Brazil.

shape, but also by environmental factors such as electric and magnetic fields. It is also defined by many-body effects like electron–electron interaction, which may become even more important than the confinement itself. In all cases, a correct description of the physical properties of the problem requires the system wave function to reflect the presence of both confinement, internal and external interactions, and the corresponding boundary conditions, in an appropriate way. We should also mention the existence of other confined systems, for example, those constituted by phonons [6], plasmons [7], or confined bosonic gases [8].

Low-dimensional electronic gases are defined in semiconductor structures when the bulk translation symmetry is broken in one or more spatial dimensions, giving origin to two-dimensional (2D) (quantum wells), 1D (quantum wires), or 0D (quantum dots) systems. In such structures, the charged carriers lose, the characteristic of being delocalized in both three spatial dimensions and become confined, for some interval of energy, in regions of mesoscopic sizes inside the crystal. This fact transforms the continuum energy bands into broken sub-bands or even into fully discretized energy states, as occurs in semiconductor quantum dots (QDs), which are the main type of confined system to be addressed in this work.

An important point to bear in mind is that the usual charging model [9–12], which reduces the electron–electron interaction inside the dot to a constant proportional to its electronic occupation, is reasonably able to reproduce the experimental findings for metallic dots. However, to obtain a more realistic description of many-particle semiconductor dots, their relatively lower electronic density makes it imperative to consider the electron–electron interaction microscopically. In strong confinement regimes, this interaction may even be included in a perturbative scheme.

Various approaches have been used to deal with many-particle QDs: charging model, correlated electron model [13], Green functions [14], Lanczos algorithm [15], Monte Carlo method [16], Hartree–Fock (HF) calculations [17–20] and density functional theory (DFT) [21]. It is useful to emphasize that not only the many-body effects, but also the spatial symmetry (geometric confinement), become indispensable ingredients for a precise determination of quantum effects in the electronic structure of semiconductor QDs.

Among the several kinds of geometries confining a QD, perhaps the most common is a 2D one defined by a parabolic potential [22–26]. In the present work, we will consider a 3D QD defined by an infinite spherical potential. The former describes QDs lithographically defined in the plane of a 2D electron gas, while the latter describes nanocrystal QDs grown inside glass matrices. A recent experiment has identified atom-like electronic states in nanocrystal QDs [27]. Some of the commonly studied topics in 3D QDs are the formation of energy shells in their spectra [28], the control of electronic correlations [29], the formation of Wigner molecules in the system [30], and the influence of the Coulomb interaction in their spectra [31, 32]. In such spherically defined 3D QD, both spin and orbital angular momenta are good quantum numbers, and the many-particle eigenstates can be labeled according to the usual **LS**-coupling scheme [33], where the analytic many-particle eigenstates are given as a sum over appropriate Slater determinants. However, to deal with QDs having higher occupation, the **LS**-coupling scheme is no longer appropriate. Therefore, we have chosen to use the Roothaan and Pople–Nesbet matrix formulations [34] of the single determinant self-consistent HF formalism, respectively, appropriate for handling closed-shell and open-shell configurations. With them, we also calculate the QD addition spectrum and show how a magnetic field is able to violate Hund's rule. Here we consider a QD populated with up to $N = 40$ electrons under the presence of a magnetic field, and expand our basis in a set of properly optimized Gaussian functions. In principle, one could also include spin-orbit coupling in the model, where L and S would then no longer be good quantum numbers, but for an infinite spherical potential such coupling yields no contribution to the total energy of the system.

The present work is organized as follows. In Section 2, for completeness, and to introduce our notation, both restricted and unrestricted formalisms are resumed. Section 3 shows the Hamiltonian model and discusses how both QD chemical potential and charging energy are calculated. We also present details of how the inclusion of a magnetic field changes the previous formalisms, as well as how the Gaussian basis set is constructed. Section 4 gives our results, and Section 5 presents our conclusions.

2. Theoretical Method

The HF approach assumes that the N-electron ground state of an interacting system is given by

the single Slater determinant $|\Psi_0\rangle = |\chi_1\chi_2 \cdots \chi_a\chi_b \cdots \chi_{N-1}\chi_N\rangle$, where the set of optimized spin orbitals $\{\chi_a|a = 1 \ldots N\}$ is obtained by the minimization of the total energy E_0 of such a state:

$$E_0 = \langle\Psi_0|H|\Psi_0\rangle = \sum_a h_{aa} + \frac{1}{2}\sum_{a,b}[J_{ab} - K_{ab}], \quad (1)$$

where the kinetic h_{aa}, direct J_{ab}, and exchange K_{ab} contributions to E_0 are well known [34]. The minimization of this equation yields the self-consistent integro-differential HF equation, $f|\chi_a\rangle = \varepsilon_a|\chi_a\rangle$, where the Fock operator is $f = h_a + \Sigma_b[J_b - K_b]$. The model we use for the confinement potential $V(\mathbf{r})$, which is present in h, is an infinite spherical barrier. Also, the kinetic (direct and exchange) term present in h (J and K) is parametrized by the effective electron mass m (dielectric constant ξ) of the material. Throughout this work, we will use the well-known [34] matrix formalisms for solving the HF equation, i.e., Roothaan [restricted HF (RHF), for closed-shell systems] and Pople–Nesbet [unrestricted HF (UHF), for open-shell systems].

In the RHF approach, both α (up) and β (down) spin functions are restricted to have the same spatial component, i.e., $\chi_i(\mathbf{x}) = \{\psi_j(\mathbf{r})\alpha(\omega), \psi_j(\mathbf{r})\beta(\omega)\}$. The doubly occupied spatial orbitals ψ_j, describing a closed-shell system having total angular momenta $J = L = S = 0$, are obtained via $f_{\mathrm{RHF}}|\psi_a\rangle = \varepsilon_a|\psi_a\rangle$, where the Fock operator reads $f_{\mathrm{RHF}} = h_a + \Sigma_b^{N/2}[2J_b - K_b]$. By expanding the set $\{\psi_i|i = 1 \ldots k\}$ in a set of known basis functions $\{\phi_\nu|\nu = 1 \ldots k\}$,

$$\psi_i = \sum_\nu C_{\nu i}\phi_\nu, \quad (2)$$

one obtains the characteristic Roothaan equation, $\mathbf{FC} = \mathbf{SC}\varepsilon$. Here, $\mathbf{S}$ is the overlap matrix between the basis functions, whose elements are $S_{\mu\nu} = \langle\phi_\mu|\phi_\nu\rangle$, $\mathbf{C}$ is the matrix of the expansion coefficients $C_{\nu i}$, whose columns describe each spatial orbital ψ_i, ε is the diagonal matrix of the orbital energies ε_i, and $\mathbf{F}$ is the matrix of the Fock operator, whose elements are $F_{\mu\nu} = \langle\phi_\mu|f_{\mathrm{RHF}}|\phi_\nu\rangle$.

The UHF approach relies on allowing the α and β spin functions to have different spatial components, i.e., $\chi_i(\mathbf{x}) = \{\psi_j^\alpha(\mathbf{r})\alpha(\omega), \psi_j^\beta(\mathbf{r})\beta(\omega)\}$, where spin-up (spin-down) electrons are described by the spatial orbitals ψ_j^α (ψ_j^β). These spatial orbitals describing an open-shell system no longer necessarily yield eigenstates having defined L and S values. They are obtained via $f_{\mathrm{UHF}}^{\alpha/\beta}|\psi_j^{\alpha/\beta}\rangle = \varepsilon_j^{\alpha/\beta}|\psi_j^{\alpha/\beta}\rangle$, where the Fock operator now becomes $f_{\mathrm{UHF}}^{\alpha/\beta} = h_j + \Sigma_a^{N^{\alpha/\beta}}[J_a^{\alpha/\beta} - K_a^{\alpha/\beta}] + \Sigma_a^{N^{\beta/\alpha}} J_a^{\beta/\alpha}$. By distinctly expanding the spatial orbitals ψ^α and ψ^β in the same set of known basis functions ϕ_ν,

$$\psi_i^{\alpha/\beta} = \sum_\nu C_{\nu i}^{\alpha/\beta}\phi_\nu, \quad (3)$$

one gets the characteristic Pople–Nesbet equation, $\mathbf{F}^{\alpha/\beta}\mathbf{C}^{\alpha/\beta} = \mathbf{SC}^{\alpha/\beta}\varepsilon^{\alpha/\beta}$. Now, $\mathbf{S}$ represents again the overlap matrix between the basis functions, $\mathbf{C}^{\alpha/\beta}$ is the matrix of the expansion coefficients $C_{\nu i}^{\alpha/\beta}$, $\varepsilon^{\alpha/\beta}$ is the matrix of the orbital energies $\varepsilon_i^{\alpha/\beta}$, and $\mathbf{F}^{\alpha/\beta}$ is the matrix of the Fock operator, whose elements now become $F_{\mu\nu}^{\alpha/\beta} = \langle\phi_\mu|f_{\mathrm{UHF}}^{\alpha/\beta}|\phi_\nu\rangle$.

As already mentioned, one disadvantage of the UHF approach is that unrestricted functions, in general, are not eigenstates of the total spin S, even though they have defined M_S values. However, one may use the expression [34]

$$\langle S^2\rangle_{\mathrm{UHF}} = \left(\frac{N^\alpha - N^\beta}{2}\right)\left(\frac{N^\alpha - N^\beta}{2} + 1\right) + N^\beta - \sum_a^{N^\alpha}\sum_b^{N^\beta}\left[\sum_{\mu,\nu} C_{\mu a}^{\alpha *} C_{\nu b}^{\beta} S_{\mu\nu}\right]^2 \quad (4)$$

to get an estimative for S, while M_S is obtained from

$$\langle M_S\rangle_{\mathrm{UHF}} = \frac{1}{2}\sum_{\mu,\nu}\left(\sum_a^{N^\alpha} C_{\mu a}^{\alpha} C_{\nu a}^{\alpha *} - \sum_a^{N^\beta} C_{\mu a}^{\beta} C_{\nu a}^{\beta *}\right)S_{\mu\nu}, \quad (5)$$

where N_α (N_β) is the number of spin up (down) electrons, with $N = N_\alpha + N_\beta$. In general, the expected value of S will be higher than expected because of contamination from other symmetries. For details concerning both RHF and UHF equations, as well as the iterative procedure for their solution until a converged ground-state energy is obtained, see Ref. [34].

3. Spherical Quantum Dot

As an application of both RHF and UHF formalisms, we consider a QD with radius R_0 confined by an infinite spherical potential in the presence of a magnetic field $\mathbf{B} = B_0(0, 0, 1)$ that can be populated with up to 40 electrons. The single-particle Hamiltonian has the form

$$H_0 = \frac{\hbar^2}{2m}\left(-i\nabla + \frac{e}{\hbar c}\mathbf{A}\right)^2 + g\frac{\mu_B}{\hbar}\mathbf{B}\cdot\mathbf{S}, \quad (6)$$

where $\mu_B = e\hbar/(2m_0c)$ is the Bohr magneton, g is the bulk g-factor, and the vector potential is used in the symmetric gauge $\mathbf{A} = (\mathbf{B} \times \mathbf{r})/2$. By using atomic units, $E_{R_y} = e^2/(2a_0)$ for energy and $a_0 = \hbar^2/(m_0e^2)$ for length, the Hamiltonian H_0 can be written as

$$H_0 = \frac{1}{\tilde{m}}\frac{a_0^2}{R_0^2}\left[-\frac{1}{x^2}\frac{\partial}{\partial x}\left(x^2\frac{\partial}{\partial x}\right) + \frac{\mathbf{L}^2}{x^2} + \frac{R_0^2}{2l_B^2}(L_Z + \tilde{m}gM_S) + \frac{R_0^4}{4l_B^4}x^2\sin^2(\theta)\right], \quad (7)$$

where $\tilde{m} = m/m_0$, $l_B = \sqrt{\hbar c/(eB_0)}$ is the magnetic length, and $x = r/R_0$ is a dimensionless variable. Without a magnetic field, the normalized spatial eigenfunctions of H_0 are given by

$$\phi_\nu(\mathbf{r}) = \phi_{n,l,m_l}(x, \theta, \phi) = \left[\frac{2}{R_0^3}\frac{1}{[j_{l+1}(\alpha_{nl})]^2}\right]^{1/2} j_l(\alpha_{nl}x)Y_{l,m_l}(\theta, \phi). \quad (8)$$

The boundary condition at the surface $r = R_0$ determines α_{nl} as the nth zero of the spherical Bessel function $j_l(\alpha_{nl}x)$; also, the spherical harmonic $Y_{l,m_l}(\theta, \phi)$ is the well-known eigenstate of $\mathbf{L}^2$ and L_Z.

The Hamiltonian for the electron–electron interaction, in units of E_{Ry}, has the form

$$H_{ee} = \frac{2}{\xi}\frac{a_0}{R_0}\frac{1}{|\mathbf{x}_1 - \mathbf{x}_2|}. \quad (9)$$

By using the multipole expansion,

$$\frac{1}{|\mathbf{x}_1 - \mathbf{x}_2|} = \sum_{\kappa=0}^{\infty}\frac{4\pi}{2\kappa+1}\frac{x_<^\kappa}{x_>^{\kappa+1}}\sum_{m_\kappa=-\kappa}^{\kappa}(-1)^{m_\kappa}Y_{\kappa,m_\kappa}(\theta_1, \phi_1)Y_{\kappa,-m_\kappa}(\theta_2, \phi_2), \quad (10)$$

the entire angular part of the problem can be solved analytically and, after inserted into our numerical code, we are left to solve only the radial degree of freedom.

Without magnetic field, we take into account in Eqs. (2) and (3) the spatial orbitals that define the six lowest energy shells (1s, 1p, 1d, 2s, 1f, 2p) under this symmetry [35]. Therefore, the index $\nu \equiv n, l, m_l$ can assume up to 40 (20 spin-up and 20 spin-down) possible values for the states within those shells. Certainly, the inclusion of a magnetic field lifts both the spin and orbital degeneracies of those states. In our application, we shall consider two possible materials forming the QD, i.e., GaAs (wide-gap material) and InSb (narrow-gap material), whose defining parameters are $\tilde{m} = 0.065$, $g = 0.45$, and $\xi = 12.65$ for GaAs, and $\tilde{m} = 0.013$, $g = -53.1$, and $\xi = 16.5$ for InSb.

Because of the presence of a magnetic field, some modifications of both RHF and UHF expressions must be made. In the Roothaan approach, the quadratic term in B_0 ($\sim l_B^{-4}$) must be added to the single-particle contribution present in h_{aa}; the linear terms in $B_0(\sim l_B^{-2})$ are zero for a closed-shell configuration, thus yielding no contribution. However, all terms proportional to B_0 have to be considered in the Pople–Nesbet formalism, since then one deals with an open shell configuration. Both linear ($\sim B_0L_Z$) and quadratic terms can be straightly added to the definitions of h_{aa}. In contrast, the inclusion of the spin-dependent linear term ($\sim B_0M_S$) in h_{aa} will impose the kinetic matrix $T_{\mu\nu}$, which together with the electron–electron matrix $G_{\mu\nu}^{\alpha/\beta}$ defines the Fock matrix via $F_{\mu\nu}^{\alpha/\beta} = T_{\mu\nu} + G_{\mu\nu}^{\alpha/\beta}$, to be decomposed in its components as $T_{\mu\nu}^{\alpha/\beta}$ (as occurs with $G_{\mu\nu}^{\alpha/\beta}$). Note that the Fock matrix in the Roothaan formalism is $F_{\mu\nu} = T_{\mu\nu} + G_{\mu\nu}$.

The last important detail in our approach refers to the orbital basis $\{\phi_\nu|\nu = 1 \ldots k\}$ used in our calculations. Instead of the spherical Bessel functions of Eq. (8), the radial part of each orbital is decomposed in a sum involving five Gaussians confined to a sphere of radius R_0, while the angular part is maintained as defined by its symmetry. So, we change the basis in Eq. (8) to

$$\phi_{n,l,m_l}(x, \theta, \phi) = N_{nl}(1-x)^n x^l \prod_{i=1}^{n-1} \times (\tilde{\alpha}_{il} - x)\sum_{k=1}^{5} V_k e^{-D_k R_0^2 x^2} Y_{l,m_l}(\theta, \phi), \quad (11)$$

where N_{nl} is the orbital normalization, the polynomial in $(1 - x)$ satisfies the boundary condition at $x = 1$ ($r = R_0$), and the polynomial in x makes the functions having $l > 0$ zero at the origin $x = 0$; also, the product in $(\tilde{\alpha}_{il} - x)$ makes the function zero at the zeros $\tilde{\alpha}_{il}$ of the respective spherical Bessel func-

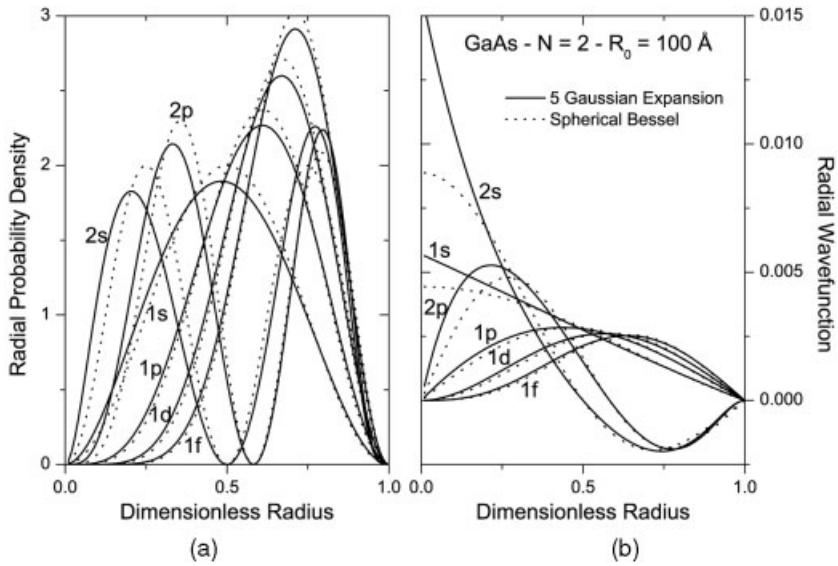

FIGURE 1. Comparison between the expanded Gaussian basis sets used in our calculations and the respective exact spherical Bessel functions, for a GaAs QD having $N = 2$ and $R_0 = 100$ Å. (a) Probability densities. (b) Wave functions. Agreement is good for all orbitals except very closed to the origin for *s*-states.

tion transposed to the interval $0 \leq x \leq 1$, and the last sum involves an expansion in five Gaussians. For $N \leq 40$, a higher number of Gaussians in the expansion does not show any improvement on our results. The coefficients V_k as well as the exponents D_k are determined for each value of R_0, and are obtained by using the condition of maximizing the superposition between Eq. (11) and the respective spherical Bessel function. Once V_k and D_k are determined and the basis is found, we run our RHF (UHF) code for given values of R_0 and N, and find the parameters $C_{\nu i}$ ($C_{\nu i}^{\alpha/\beta}$) that better describe Eq. (2) [Eq. (3)] and yielding the converged energy within the RHF (UHF) formalism.

Finally, we calculate two closely related quantities that give interesting information on the charging processes of a confined system. The first is the QD chemical potential, $\mu_{\text{dot}}(N)$, which yields the energy difference between two successive ground states, and can be calculated as

$$\mu_{\text{dot}}(N) = E_0(N) - E_0(N-1). \tag{12}$$

The second is the QD charging energy, $E_{\text{char}}(N)$, which yields the energy cost for the addition of an extra electron to the system,

$$E_{\text{char}}(N) = I(N) - A(N) = E_0(N+1) - 2E_0(N) + E_0(N-1). \tag{13}$$

Here, $I(N) = E_0(N-1) - E_0(N)$ is the ionization potential, while $A(N) = E_0(N) - E_0(N+1)$ is the electronic affinity. It becomes clear, from these two equations, that $E_{\text{char}}(N) = \mu_{\text{dot}}(N+1) - \mu_{\text{dot}}(N)$.

4. Results

Figure 1 compares the exact orbitals described by the spherical Bessel functions of Eq. (8) and the expansions involving the Gaussians of Eq. (11) used in our calculations for a GaAs QD of $N = 2$ and $R_0 = 100$ Å. Figure 1(b) shows the radial wave functions, while Figure 1(a) shows the radial probability densities. Although one can observe a difference in the *s*-wave functions, near $x = 0$, their probability densities are reasonable in that region. For any other occupation and radius, as well as for InSb QDs, this same feature regarding *s*-orbitals is found. Table I shows the optimized coefficients and exponents for the five Gaussians related to the six orbitals taken into account. The factor 10^{-4} in all exponents cancels the term R_0^2 in Eq. (11). Besides, all exponents related to any orbital having $n = 2$ are negative since there are regions where those wavefunctions possess negative values.

Figure 2 shows the results of a RHF–Roothaan calculation. Figure 2(a) presents the ground-state energy as a function of the radius for a GaAs QD

TABLE I

Values of the five coefficients and exponents that optimize the set of Gaussians used in the expansions for the six orbitals considered in this work.

Orbital	V_1, $D_1(10^{-4})$	V_2, $D_2(10^{-4})$	V_3, $D_3(10^{-4})$	V_4, $D_4(10^{-4})$	V_5, $D_5(10^{-4})$
1*s*	0.3229, 0.003	0.2353, 0.328	0.4554, 0.043	0.9069, 0.330	0.8317, 0.006
1*p*	0.5902, 0.762	0.0646, 0.564	0.5941, 0.447	0.4599, 0.350	0.9727, 0.724
1*d*	0.7301, 1.120	0.9570, 0.915	0.8227, 1.620	0.1950, 0.492	0.4194, 1.100
2*s*	0.4823, −2.260	0.9875, −2.440	0.1082, −1.530	0.4006, −2.840	0.0342, −2.260
1*f*	0.6377, 1.500	0.4539, 1.920	0.9730, 1.440	0.4921, 1.610	0.5498, 1.360
2*p*	0.8513, −1.420	0.0413, −3.720	0.0565, −0.401	0.8797, −1.410	0.0457, −1.700

populated with 2, 8, and 18 electrons, while Figure 2(b) shows the same, but for a InSb QD populated with 2, 34, and 40 electrons. These five distinct values, plus $N = 20$, are the successive magic numbers for the closed-shell configurations at this symmetry. In both QDs, note that the kinetic energy is much higher and totally dominates the Coulomb energy at smaller radii. Thus, the energies related to different N values are more distant from each other. At larger radii, or at smaller electronic density, the electron–electron interaction becomes more important and the energy separation decreases. In the insets, which show a zoom at larger radii, we analyze the influence of the magnetic field on the system-shell configuration. For every N, the curves for increasing energy ordering refer to fields of 0, 2, 5, 8, and 10 T, even though we have only labeled the cases with $N = 18$ and $N = 40$; for $N = 2$, the

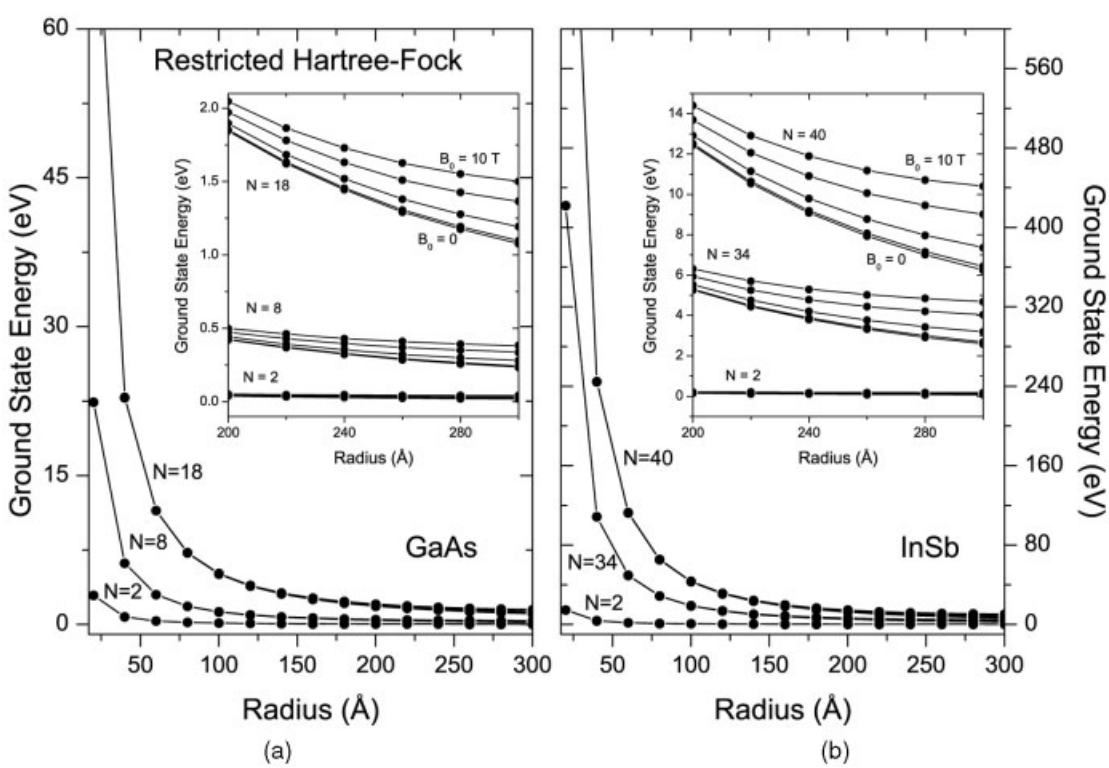

FIGURE 2. Restricted ground-state energies for a GaAs (a) and InSb (b) QD populated with $N = 2$, 8, and 18 ($N = 2$, 34, and 40) electrons. The Coulomb contribution is more important at larger radii. (Insets) Influence of a magnetic field in the system, where one can see that even in a closed-shell configuration having $L = S = 0$, the presence of the field is visible due to the diamagnetic term.

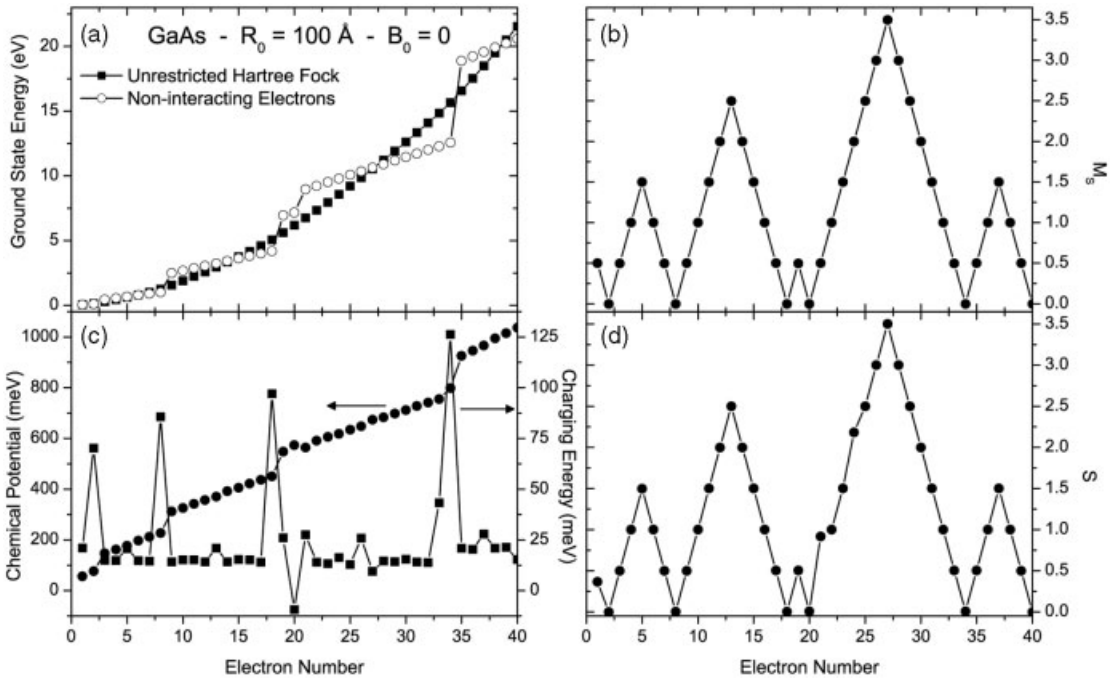

FIGURE 3. Unrestricted ground-state energies for a $R_0 = 100$ Å GaAs QD without magnetic field. (a) Comparison of unrestricted and noninteracting energies, where the QD energy shell structure is visible. (c) QD chemical potential (left scale) and charging energy (right scale); the former displays abrupt change every time that a new shell starts to be populated, while the latter presents larger (smaller) peaks when a shell is filled (half-filled), a direct consequence of Hund's rule. *N*-evolution of the expected values of total spin *S* (d) and its projection M_S (b).

presence of the magnetic field is imperceptible. As also expected, due to its large *g*-factor, the Zeeman splitting is much higher for the InSb QD (observe the different energy scales in the insets). Most interesting is the fact that even for a closed-shell configuration, where $L = S = 0$, the influence of the quadratic field (diamagnetic term) of Eq. (7), which is the only nonzero contribution in the restricted case, becomes important mainly for higher occupation numbers and fields, as well as at larger radii (note that there is almost no difference between 0 and 2 T for any *N*).

To study spectra for any occupation, Figure 3 shows the results of a UHF–Pople–Nesbet calculation for a GaAs QD having $R_0 = 100$ Å, and without a magnetic field. Figure 3(a) compares the UHF results with the noninteracting electron case, where the energy shell structure is clear for $N = 2$, 8, 18, 20, 34, and 40. Note that the electron–electron interaction causes the energy of a QD, whose occupation corresponds to a shell less (more) than half-filled, to be decreased (increased) with respect to the noninteracting case. When this occupation corresponds exactly to half-filled cases ($N = 5$, 13, 27, and 37), the interacting energy is approximately equal to the noninteracting energy.

Figure 3(c) shows both QD chemical potential [left scale, Eq. (12)] and charging energy [right scale, Eq. (13)], where the respective values of E_0 are obtained from the unrestricted calculation presented in Figure 3(a). Observe that μ_{dot} increases linearly as the occupation becomes higher inside a given shell. When this shell is totally filled, there is an abrupt change in μ_{dot}, indicating that the following shell begins its occupation; observe that the higher the occupation, the larger the change. An anomalous behavior appears to occur for the 2*s* shell, whose μ_{dot} value is larger than the one for the 1*f* shell (that has higher energy). The charging energy is another way to verify not only the presence of shell structure for the spectrum, but also the validity of Hund's rule for the filling of such shells. In principle, E_{char} must present larger (smaller) peaks when the total (half) occupation of a given shell is achieved; the first fact (larger peaks) is due to the higher difficulty to the addition of an extra electron to a QD when a filled shell state is reached. The second fact (smaller peaks) refers to Hund's

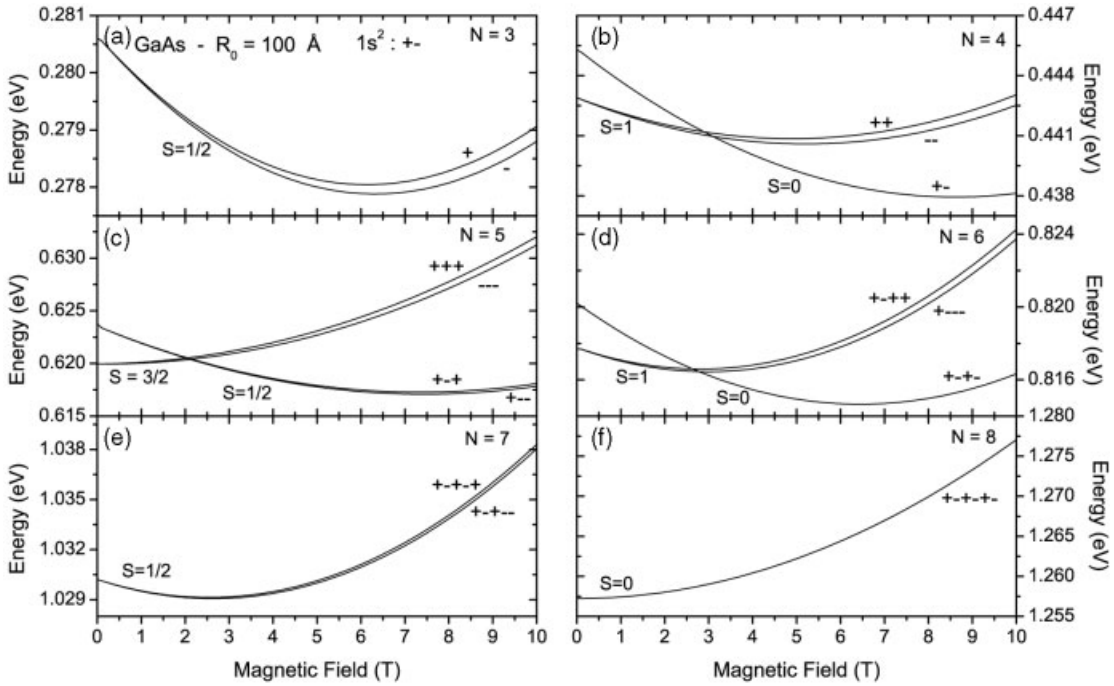

FIGURE 4. (a)–(f) Violation of Hund's rule induced by magnetic field in the $R_0 = 100$ Å GaAs QD of Fig. 3. Successive occupation (indicated in upper right corner of each panel) of the 1*p* shell, assumes that the 1*s* shell remains populated by one spin-up and one spin-down electron. The possible spin configurations for a given *N* are indicated by + (spin-up) and − (spin-down). For $B_0 = 0$, the ground-state spin sequence is 1/2–1–3/2–1–1/2–0, while at fields higher than 3 T it changes to 1/2–0–1/2–0–1/2–0. It is interesting to observe that a magnetic field is able to shift triplet and quartet states of *p*-shells to higher energies.

rule, which establishes that electrons must be added to the system with their spins parallel, until all possible orbitals inside a given shell are occupied; this makes the total energy of the system smaller, since this procedure maximizes the negative exchange contribution. However, some violations of this rule can be verified in E_{char}: the smaller peak of $N = 27$ occurs here at $N = 26$, and the larger peak of $N = 20$ has a negative value.

Figure 3(d) and (b) shows, respectively, the evolution of the total spin S and its projection M_S as a function of the QD population, calculated from Eqs. (4) and (5) for the unrestricted energies. Note that, without the magnetic field, Hund's rule appears to be followed for all states with up to 40 electrons. The M_S expected value oscillates from 0 in a filled shell to its maximum in a half-filled shell, when it starts to decrease again on the way to the closing of the shell; the maxima are $M_S = 1/2, 3/2, 5/2$, and $7/2$ for *s*, *p*, *d*, and *f* shells, respectively. The S expected value yielded by the unrestricted formalism is also very reasonable; discrepancies are only observed at $N = 24$, where $S > 2$, and at $N = 21$, where $S > 1/2$. We believe that both discrepancies related to the 2*s* shell or to its surroundings (i.e., μ_{dot} larger than the one of 1*f* shell, negative peak for $N = 20$ in E_{char}, and almost doubled S expected value for $N = 21$) are caused by the unsatisfactory Gaussian reproduction of this orbital close to the origin, as observed in Figure 1. These same qualitative results are observed for an InSb QD without a magnetic field.

By focusing on the 1*p* shell, we show in Figure 4 for the same QD illustrated in Figure 3, how a finite magnetic field is able to violate Hund's rule in the system. Figure 4 [left to right (a) to (b), (c) to (d), and (e) to (f), as well as from top to bottom (a) to (e) and (b) to (f)] shows the successive ground-state energies from $N = 3$ to $N = 8$ as this shell is filled, always considering that the 1*s* shell remains fully occupied by two electrons, one spin-up and one spin-down; the distinct possible spin configurations for each N are indicated by + (spin-up) and − (spin-down). In addition to the small Zeeman effect present in all occupations, there is a change of ground-state spins at $N = 4$, 5, and 6 as the field is

increased. Note that at zero field, the spin sequence is 1/2–1–3/2–1–1/2–0; in a field above 3 T, it becomes 1/2–0–1/2–0–1/2–0, showing that quartets and triplets are shifted to higher energies by the magnetic field, so that the ground state of the system begins to oscillate only between singlets and doublets at high fields as N increases. When this $1p$ shell is half-filled ($N = 5$), the ground state goes from a quartet to a doublet at $B_0 \simeq 2$ T; when it has one electron more ($N = 6$) or less ($N = 4$) than that, it goes from a triplet to a singlet at $B_0 \simeq 3$ T.

At last, we have compared the results from both RHF and UHF self-consistent matrix formulations with those obtained [36] from the **LS**-coupling scheme, where a GaAs QD having $R_0 = 90$ Å was considered, and the quadratic term in B_0 was neglected, since only small magnetic fields were considered. Also, only $N = 2$ and $N = 3$ occupations were calculated, since the states were constructed analytically (not only a single Slater determinant), and the electron–electron interaction was included by using perturbation theory, which is justified at such radius. At zero field, the energies for $N = 2$ are 16.5 meV (**LS**) and 16.1 meV (RHF), while for $N = 3$ they are 34.8 meV (**LS**) and 33.9 meV (UHF). Therefore, both Roothaan and Pople–Nesbet formalisms indeed give smaller ground-state energies than are obtained with the **LS** perturbative scheme. We have also checked the validity of neglecting the diamagnetic term (quadratic in B_0) for fields smaller than 2 T. We may emphasize here that, in principle, a disadvantage of the UHF approach is that one cannot always rely on the expected values for L and S in a given QD state. In contrast, the applicability of the **LS** scheme is cumbersome and becomes very complicated to handle analytically as the QD occupation increases.

5. Conclusions

We have shown how the mean-field Roothaan and Pople–Nesbet formalisms applied to a spherical quantum dot confined system under magnetic field yield a fairly good description of its energy shell structure. For a maximum population of 40 electrons considered in the present study, the appropriate Gaussian basis set for each radius has been found. We have seen how the magnetic field influences the total energy of ground states even in closed-shell configurations. We have also shown how both chemical potential and charging energy reproduce the closing and half-closing structures of the quantum dot energy shells. With the calculation of the total spin expected value for each occupation, in a given radius, we have observed that Hund's rule is satisfied at zero field. However, under a finite magnetic field, we have shown that its applicability is violated and, at given values of the field, which depend on quantum dot radius and material parameters, transitions occur that change a given ground-state symmetry.

An experimental comparison with our results would be valuable. However, experiments in InSb or GaAs nanocrystals (spherical confinement) are not easy to implement (see, e.g., the discussion for InSb in Refs. [37] and [38] and references therein). In contrast, experiments in GaAs have been extensively done but in 2D electron gases (etching techniques). Most experiments involving 3D nanocrystals (see, e.g., Ref. [27] and references therein), where our present model would apply, have used other materials: CdTe, CdSe, PbTe, and CdS in the II–VI group, as well as InAs, InP, GaP, and GaN in the III–V group. Consequently, there are no available experimental values for our systems (at the specific quantities calculated here), so that we could only compare our RFH and UHF models with a previous work based on the LS-coupling scheme. It would be interesting to carry out experiments involving these nanocrystals to obtain further information on the applicability of RHF and UHF approaches to quantum dot confined systems.

ACKNOWLEDGMENTS

The authors are indebted to C. Trallero-Giner for discussions on this subject.

References

1. Jaskólski, W. Phys Rep 1996, 271, 1.
2. Connerade, J. P.; Dolmatov, V. K.; Lakshmit, P. A. J Phys B: At Mol Opt Phys 2000, 33, 251.
3. Rivelino, R.; Vianna, J. D. M. J Phys B: At Mol Opt Phys 2001, 34, L645.
4. Bielinska-Waz, D.; Karkowski, J.; Diercksen, G. H. F. J Phys B: At Mol Opt Phys 2001, 34, 1987.
5. Beekman, R. A.; Roussel, M. R.; Wilson, P. J. Phys Rev A 1999, 59, 503.
6. Grinberg, M.; Jaskólski, W.; Koepke, C.; Planelles, J.; Janowicz, M. Phys Rev B 1994, 50, 6504.
7. Gudmundson, V.; Gerhardts, R. R. Phys Rev B 1991, 43, 12098.
8. Grossmann, M.; Holthaus, M. Z Phys B 1995, 97, 319.

9. Averin, D. V.; Korothov, A. N.; Likharev, K. K. Phys Rev B 1991, 44, 6199.
10. Beenakker, C. W. J. Phys Rev B 1991, 44, 1646.
11. Grabert, H. Z Phys B 1991, 85, 319.
12. Kouwenhoven, L. P.; Vaart, N. C.; van der Johnson, A. T.; Kool, W.; Harmans, C. J. P. M.; Williamson, J. G.; Staring, A. A. M.; Foxon, C. T. Z Phys B 1991, 85, 367.
13. Weinmann, D.; Häusler, W.; Kramer, B. Ann Phys 1996, 5, 652.
14. Cipriani, G.; Rosa-Clot, M.; Taddei, S. Phys Rev B 2000, 61, 7536.
15. Jauregui, K.; Häusler, W.; Weinmann, D.; Kramer, B. Phys Rev B 1996, 53, R1713.
16. Harting, J.; Mülken, O.; Borrmann, P. Phys Rev B 2000, 62, 10207.
17. Pfannkuche, D.; Gudmundsson, V.; Maksym, P. A. Phys Rev B 1993, 47, 2244.
18. Alhassid, Y.; Malhotra, S. Phys Rev B 2002, 66, 245313.
19. Reusch, B.; Grabert, H. Phys Rev B 2003, 68, 045309.
20. Bednarek, S.; Szafran, B.; Adamowski, J. Phys Rev B 1999, 59, 13036.
21. Ferconi, M.; Vignale, G. Phys Rev B 1994, 50, 14722.
22. Costa, L. S.; Prudente, F. V.; Acioli, P. H.; Soares Neto, J. J.; Vianna, J. D. M. J Phys B: At Mol Opt Phys 1999, 32, 1.
23. Ashoori, R. C.; Stormer, H. L.; Weiner, J. S.; Pfeiffer, L. N.; Baldwin, K. W.; West, K. W. Phys Rev Lett 1983, 71, 613.
24. Tarucha, S.; Austing, D. G.; Honda, T.; van der Hage, R. J.; Kouwenhoven, L. P. Phys Rev Lett 1996, 77, 3613.
25. Lockwood, D. J.; Hawrylak, P.; Wang, P. D.; Torres, C. M. S.; Pinczuk, A.; Dennis, B. S. Phys Rev Lett 1996, 77, 354.
26. Hawrylak, P.; Gould, C.; Sachradja, A.; Feng, Y.; Wasilewski, Z. Phys Rev B 1999, 59, 2801.
27. Banin, U.; Cao, Y.; Katz, D.; Millo, O. Nature 1999, 400, 542.
28. Heiss, W. D.; Nazmitdinov, R. G. Phys Rev B 1997, 55, 16310.
29. Lozovik, Y. E.; Volkov, S. Y. Phys Sol Stat 2003, 45, 364.
30. Sundqvist, P. A.; Volkov, S. Y.; Lozovik, Y. E.; Willander, M. Phys Rev B 2002, 66, 075335.
31. Pandey, R. K.; Harbola, M. K.; Singh, V. A. Phys Rev B 2003, 67, 075315.
32. Szafran, B.; Adamowski, J.; Bednarek, S. Physica E 1999, 4, 1.
33. Condon, E. U.; Shortley, G. H. The Theory of Atomic Spectra; Cambridge University Press: London, 1977.
34. Szabo, A.; Ostlund, N. S. Modern Quantum Chemistry: Introduction to Advanced Electronic Structure Theory; Dover: New York, 1999.
35. Fetter, A. L.; Walecka, J. D. Quantum Theory of Many-Particle Systems; McGraw-Hill: New York, 1971.
36. Destefani, C. F.; Marques, G. E.; Trallero-Giner, C. Phys Rev B 2002, 65, 235314.
37. Li, B. Y.; Wang, Z.; Duan, X.; Zhang, G.; Wang, C. Adv Mater 2001, 13, 145.
38. Efros Al, L.; Rosen, M. Annu Rev Mater Sci 2000, 30, 475.